An overview on cryogeophysics in the alpine environment

Bollettino di Geofisica Teorica ed Applicata Vol. 61, n. 1, pp. 3-22; March 2020
DOI 10.4430/bgta0304

An overview on cryogeophysics in the Alpine environment

A. Godio

Dipartimento di Ingegneria dell'Ambiente, del Territorio e delle Infrastrutture (DIATI), Politecnico di Torino, Italy

(Received: 21 February 2019; accepted: 26 September 2019)

ABSTRACT Geophysics allows us to characterise glaciers and snow properties in order to evaluate the hazard associated with the evolution of the snow/ice masses. The danger is often associated with recent phenomena of rapid deglaciation with consequent collapses of ice and rock, or with releases of water contained in the glaciers. The morphology of the rock substrate and the presence of various kinds of conduits and cavities, making up the internal hydrological network, can be investigated by seismic and radar methods; the presence of water in internal cavities of temperate glaciers can be successfully detected through georadar measurements. In the nivological context, the geophysical approach, adopting seismic and electromagnetic methods, can serve as a tool to characterise and monitor some physical properties of the snowpack. The evaluation of these parameters makes it possible to estimate the risk and the imminence associated with the snow-gliding avalanche release. We discuss the basic theoretical background of the relationships between geophysical investigated parameters and ice/snow properties; moreover, we illustrate some examples of applications of seismic and electromagnetic methods to detect the snow and ice properties in high elevation Alpine regions.

1. Introduction

In the frame of deep changes in the cryosphere of the Alps, geophysical methods are effective in identifying the main hazard elements in the Alpine environment, in addition to the geotechnical characterisation of the material composing the cryosphere (e.g. Ferrero *et al.*, 2014).

For the sake of brevity, certainly not in terms of relevance and impact on the environment, the discussion on risk assessment, associated with rock failures and debris collapses, is not considered in this context.

On the contrary, we focus on the problems related to glacial systems and the snowpack in the Alpine environment (Forte *et al.*, 2015), while discussing the different approaches of applied geophysics widely adopted in assessing hazards related to glaciers. Particularly, we deal with an overview of some challenging aspects of the application of the geophysical methods in the evaluation of hazards linked to the cryosphere in the Alpine region. The analysis of the application of seismic and electromagnetic methods offers a brief overview on the characterisation of the snow and ice properties. We also present the basic theoretical background of the relationships between the investigated geophysical parameters and ice/snow properties.

The concept of "danger", in the glaciological field, is associated with recent phenomena of rapid deglaciation with consequent collapses of ice and rock, or with releases of the water contained

in the glaciers (endoglacial lakes). Many of these phenomena are related to the alternations of periods of snow accumulation and ice formation (cold periods), with warmer periods, associated with ice-melting, infiltration of volumes of water inside the cavities, and formation of conduits and endoglacial cavities.

Because of the effect of climate change and despite a different geographical distribution of intense snowfalls with respect to the recent past, the development of new tools becomes crucial to monitor the accumulation, transport and redistribution of the snow in order to evaluate the risk of avalanches in areas not previously affected by these phenomena, or simply, to monitor the avalanche risk in well-recognised potentially risky areas. All these phenomena are monitored with different approaches, including geophysical methods, to evaluate the snow and ice thickness, or to define the mechanical properties of ice and snow (e.g. Arcone *et al.*, 1995). Active source seismic data have been previously used to investigate the firn structure, for example, in Antarctica (Picotti *et al.*, 2015) and in the Italian Alps (Godio and Rege, 2015). More recently, other authors (e.g. Diez *et al.*, 2016) investigated the firn properties and structure by using passive-source seismic arrays.

It is worth noting a number of contributions of geophysical studies in the cryosphere environment, focusing on ice and snow, concerning:

1) analysis of geometry, thickness of glacier and glacier features in the frame of glaciological and climatic studies (Stoffel and Huggel, 2012); on this, some examples are given in the studies of Eisen *et al.* (2003, 2007), Navarro *et al.* (2005), Bohleber *et al.* (2017), Picotti *et al.* (2017);
2) detection and monitoring of endoglacial features, lakes, crevasses, cavities for glaciological studies and for monitoring potential risks associated with ice collapses (e.g. Legchenko *et al.*, 2008, 2011; Vincent *et al.*, 2010, 2012; Pomeroy *et al.*, 2015). Garambois *et al.* (2016) used a combination of ground-penetrating radar (GPR) and surface nuclear magnetic resonance (SNMR) surveys to detect and monitor the evolution of a water-filled cavity within the Tête Rousse glacier (French Alps);
3) mapping the distribution of the snow cover both for snow water equivalent detection at the scale of the basin and in the frame of a mass balance analysis of glaciers (e.g. Booth *et al.*, 2013); monitoring of snow properties (density, liquid water content, etc.) for avalanche prediction (e.g. Jones, 2004).

2. The risks in deglaciated areas

One of the most obvious effects of climate change in the Alpine sites is the widespread withdrawal and disintegration of glaciers (Zemp *et al.*, 2007; Diolaiuti *et al.*, 2011). The consequences for natural hazards due to ever more rapid variations of glaciers are numerous and include the formation of marginal lakes, accumulations of volumes of endoglacial water, ice avalanches and mass movements deriving from the de-tensioning of the walls and the bedrock.

The rapid formation and growth of proglacial lakes in recent years is a global phenomenon widely observed in most of the Swiss and Italian Alps (Künzler *et al.*, 2010). Some of the lakes have become important tourist attractions, but there is considerable concern for the risks in the event of a sudden collapse of a lake triggered by ice avalanches or rock falls. The plausible

scenario envisages that, in the near future, the phenomena of deglaciation and the withdrawal of glaciers will lead to the formation of multiple marginal lakes and an intensification of flooding and outbreaks of endoglacial lakes (Frey *et al.*, 2010).

The sudden depletion of glacial lakes has been responsible for material damage to structures and the loss of life; historical examples such as that of Tète Rousse (1892) and more recently in Nepal and India, are clear testimonies. Such phenomena in the Alps generally have smaller dimensions; the glacial lakes in the Alps are generally smaller than in Nepal, although the infrastructures and settlements are much closer to the danger source. As a result, even small glacial lakes can cause considerable damage (Haeberli, 1983). All this happens in one of the most populated mountain chains in the world, where there is a constant advancing of infrastructure and settlements in high altitude Alpine areas. In the Swiss Alps, since the beginning of the "Little Ice Age", more than 100 unusual (non-periodic) floods have been observed, involving less than 40 glaciers, or about 2-3% of all Swiss glaciers (Haeberli, 1983).

The main dangerous phenomena are typical of the temperate glaciers, where the snow and ice melting is more intense, with consequent formation of surface and internal networks of water paths. The melted water, coming from the glacier, infiltrates through vertical conduits and along the endoglacial cavities network, and flowing below the glacier itself, in contact with the substratum, originates an under-glacial flow. The cavities are then progressively filled with the same melt water that created them. The collapse culminates with the failures of the vault of the cavity and, depending on the dynamics of the draining endoglacial network, the cavity can quickly deplete with the melting of the collapsed ice, leaving only a scar in the glacier. Finally, the concentration of large water volumes in cavities determines the risk of overpressure and/or breaking of the glacial margins.

A scheme of the water infiltration along vertical conduits with the formation of an endoglacial cavity is reported in Fig. 1. Moreover, a typical sequence of ice-formation is illustrated. The snow is transforming into ice along a transition zone (firn), where a gradual change of density and porosity is observed.

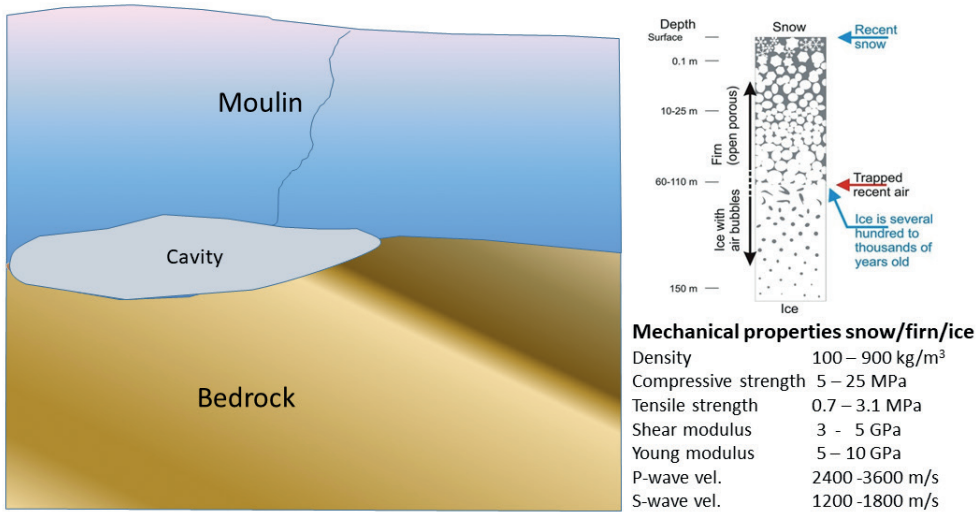

Fig. 1 - Scenario of the mechanical parameters of glacial apparatus and their influence in the analysis of roof stability of hidden cavities.

At the surface, the density of the firn is around 350 kg/m^3 and corresponds to a porosity of about 60-70%. The firn is compacted by the weight of the overlying layers and by the water vapour diffusion. The transformation of snow to ice is dominated by the rearrangement of the firn grains in order to reach a denser packing; this process predominates until a depth where the density is of about 550 kg/m^3. At greater depths, sintering and plastic deformation become the most important transformation processes. At the density of 800 kg/m^3, the pores are gradually pinched off and form bubbles in the ice.

3. Geophysics for investigating glaciers

Applied geophysics has a wide and diversified role in the characterisation of the geometry, the identification of potentially dangerous structures or volumes and the detection of the mechanical parameters of glacial masses or morainic deposits. The morphology of the rock substrate, and the presence and nature of the conduits and cavities, which constitute the internal hydrological network, can be investigated by seismic and radar methods. In particular, the presence of water in internal cavities of temperate glaciers has been successfully revealed through georadar measurements (Murray *et al.*, 2000). Combined georadar and seismic surveys provide detailed evaluations about the geometry of endoglacial features (crevasse, cavities, moulins, etc.): examples of integrated seismic and electromagnetic methods, to characterise the mechanical properties of the materials that make up the cryosphere and to identify and monitor the main endoglacial features, are widely reported in the literature (e.g. Arcone, 1996; Arcone *et al.*, 1998; Pomeroy *et al.*, 2013; Godio and Rege, 2015). These studies contributed to evaluating the dangers linked, for example, to accumulations of endoglacial water. As an example, we recall the geophysical study of the Tète Rousse glacier (Mont Blanc). The integration of georadar investigations and nuclear magnetic resonance (NMR) measurements (Legchenko *et al.*, 2014), enabled identifying a cavity of about 50,000 m^3 of water, essential for defining a glacier safety intervention with drilling and drainage operations (Vincent *et al.*, 2010).

Also in Italy, the preventive study and monitoring of glacial structures has been improved in recent years in order to identify the presence of endoglacial structures and estimate the volumes of water accumulated inside the cavities. The objective is to focus on the danger associated with the phenomena of rapid emptying of lakes or of volumes of water contained within glacial structures (Mercalli *et al.*, 2002) or in the margin of moraines. A typical example is the case of the lake at the front of the Locce glacier, in the Monte Rosa massif: a proglacial lake, known for its sudden emptying, has developed and has affected the safety of the inhabited area below (Macugnaga) (Mortara and Mercalli, 2002). In this context, a georadar survey detected the thickness of the ice in the area above the lake (Tamburini *et al.*, 2008).

By limiting the discussion to non-polar glaciers, GPR is typically applied to study the ice thickness, the accumulation distribution and the ice flow (e.g. Fischer and Kuhn, 2013). The method has also been used successfully for mapping internal features in connection to ice cores on mountain glaciers (Eisen *et al.*, 2003; Konrad *et al.*, 2013). Examples of radar investigation to map the glacier evolution are given by Carturan *et al.* (2013); their studies focused on the Careser glacier (Cevedale-Ortles group) to map the overall ice-thickness which allowed calibrating an evolution scenario of the glacier. An example of the results achieved on the Careser glacier is

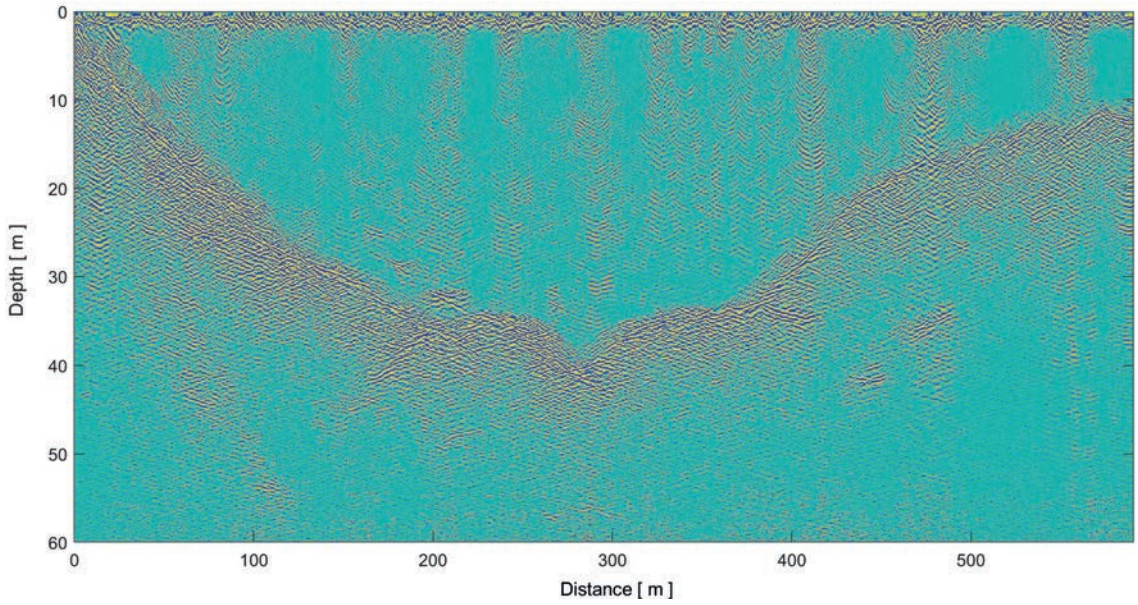

Fig. 2 - Careser glacier (Ortler massif, north-eastern Alps, Italy); example of georadar scan-B to estimate the ice thickness and delineate discontinuities owing to the presence of the crevasses and moulins, located between the coordinates 200 and 330 m.

shown in Fig. 2; the radargram shows the interface between the ice body and the bedrock; the contact deepens from the initial part, where the ice-thickness is of a few metres, up to a depth of about 40 m at the centre of the profile. Moreover, many artefacts are traced between the coordinates 200 and 300 m of the profile; those artefacts are due to the presence of endoglacial features, herein interpreted as crevasses.

Finally, seismology applied to glaciology is emerging as a new and rapidly evolving discipline. With the advent of the latest generation of seismic instrumentation, less expensive and portable, it is now possible to install sensors near and/or on the glacier. The seismic records provide important indications regarding various dynamic processes of ice, as well as the estimation of thickness and basal properties, which are challenging to study by the application of conventional techniques (Picotti *et al.*, 2015; Colgan *et al.*, 2016; Podolskiy and Walter, 2016). While ice flow events appear to be an important feature of the glacial dynamics in Antarctica, with consequent significant induced seismicity, it is not clear how widespread this kind of seismicity is in the Alpine regions. Many studies report a lack of detectable seismicity under the Alpine glaciers in the northern hemisphere (Moore *et al.*, 2013; Pomeroy *et al.*, 2013). Even if present, the basal seismicity under the Alpine glaciers cannot be correlated to the sliding, but to the opening and closing of the traction fractures in the basal areas of the glacier.

3.1. An example of glacier characterisation

In some cases, following some indicators of anomalous behaviour of the hydrological regime of the glacier, geophysical investigations are required. As an example, in the summer of 2017, an anomaly in the regular hydrology of the Chérillon Glacier (Aosta Valley, Italy) was observed, related to the sudden disappearance of a glacial stream. The survey focused on detecting possible

water retention and accumulation phenomena within the glacier. A first field survey was carried out in 2017 to observe in-situ conditions and eventual morphological evidence. No surface evidence of glacial collapse or water pocket formation was reported, but further investigations were undertaken to assess the presence of water volumes within the glacier body.

GPR data have been collected along several profiles that covered the entire north-eastern part of the glacier. The presence of buried cavities, potentially filled with water, infiltrated in the glacier through the surficial and internal network of crevasses, moulins, and fractures, has been assessed using ground probing radar with antennas at the central frequency of 200 MHz. The survey focused on the 3D detection of the cavities by a pattern of densely spaced lines (10 m apart) covering an area of about 500×500 m^2. The analysis of the collected radargrams allowed us to detect a main subglacial cavity; an example of this evidence is reported in Fig. 3. The image highlights the interface between the ice and the bedrock (letter C in Fig. 3) at the average depth of about 25-30 m and some hyperbola artefacts, indicated with letters A and B.

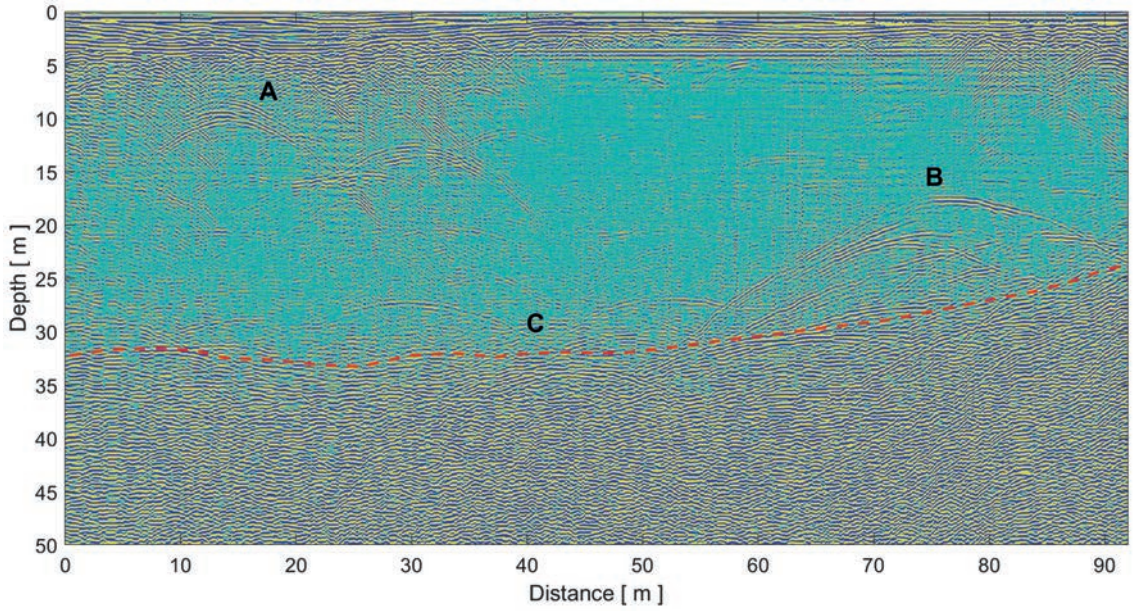

Fig. 3 - Example of radar detection of evidence of internal cavities in the glacier of Chérillon (Aosta Valley); the letter A identifies the near surface crevasses; B refers to the deeper cavities, while C is the ice-bedrock interface.

The evidence of meltwater and percolation can be observed also in some radargrams; for instance, Bohleber *et al.* (2017) reported the effects of near-surface meltwater by observing the presence of incoherent near-surface noise in 200 MHz radargrams. The noise coincides with an increased near-surface reflectivity in the 100 MHz data: this is interpreted as a backscatter due to meltwater. We observed a similar phenomenon in some radargrams of the survey over the Chérillon glacier; in Fig. 4a, we pointed out a scattering effect (indicated with letter A) located at a depth of a few metres from the surface.

In the migrated section of Fig. 4b, we highlighted the position of the zone where meltwater percolates through fractures or small crevasses. In particular, the pattern of diffraction events

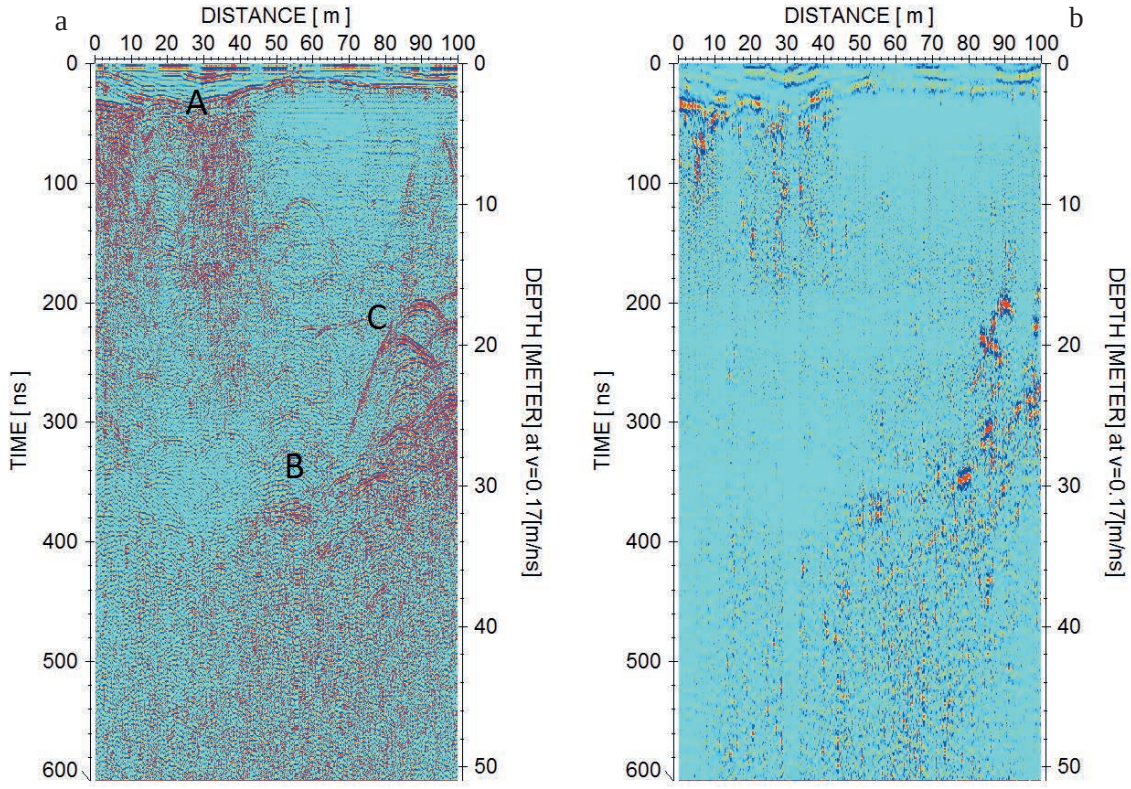

Fig. 4 - Radar data to detect the presence of buried cavities in the Chérillon glacier (survey of 2017): a) the raw radargram (B-scan) collected with antenna at central frequency of 200 MHz; b) the filtered and migrated radargram. The uppermost reflection (A) refers to the effect of the seasonal snow cover; the bedrock is only detectable in the eastern part of the section, and located at a depth between 25 and 30 m (B); the roof of the cavity is located at 15-17 m from the surface (C).

(letter A) is associated to a network of crevasses, acting as a preferential pathway of the water infiltration from the surface. This means a potential risk of accumulation of water inside the cavities (here supposed to be detected by the events indicated with letter C in Fig. 4a), even if the presence of water filling the cavity is still a matter of discussion. Stuart *et al.* (2003) have shown that englacial channels can be successfully detected using GPR. However, the attenuation effects, scattering, and ambiguities in interpreting radargrams over warm ice, suggested that such studies are most likely to be successful on polythermal or cold glaciers. A forward model procedure, providing the theoretical response, is useful to estimate whether the cavity is filled by air or water.

More recently, the theoretical response of air or water-filled cavities has been studied by means of a forward modelling procedure (Francese *et al.*, 2019). The modelling aims to estimate the nature of the material filling the cavity. In the case of an air-filled cavity, the radar signal is transmitted downwards well, while most of the wave energy is reflected back at the roof of the cavity in the case of a water-filled cavity. Francese *et al.* (2019) modelled an air-filled cavity and reported also a marked ringy effect, since the reflection is a wavetrain comprising a primary cycle and two other cycles of reverberations. The case of a cavity partially filled by water, which is the most plausible hypothesis, has also been modelled. They reported a good matching, in terms of wavelet nature and reverberation patterns, between modelled and real data.

In our case, however (Figs. 4a and 4b), the signature of the reflection event looks like a typical response of an air-filled cavity: in the case of a cavity filled by water, an inversion of polarity of the reflected signal would be expected at the interface with the cavity.

A 3D reconstruction of the shape of the ice-bedrock can be obtained by interpolating all the picked reflectors of each single transect. Fig. 5 shows the 3D image of the interface between the ice and bedrock, as interpolated from georadar data, lower surface. In particular, we have applied the migration process to the radargrams and then picked up the main continuous reflection event. This has been interpreted as the interface between ice and bedrock. Moreover, we have detected the main reflection/diffraction events, caused by the internal features of the glacier. The events are marked with red circles, and the size of each circle is qualitatively related to the size of the conduits/cavity, as assumed by the radargrams. Those events are interpreted as a network of internal conduits/cavities; the lateral coherence and the alignment of the main events offer a rough indication about the spatial connection between the cavities.

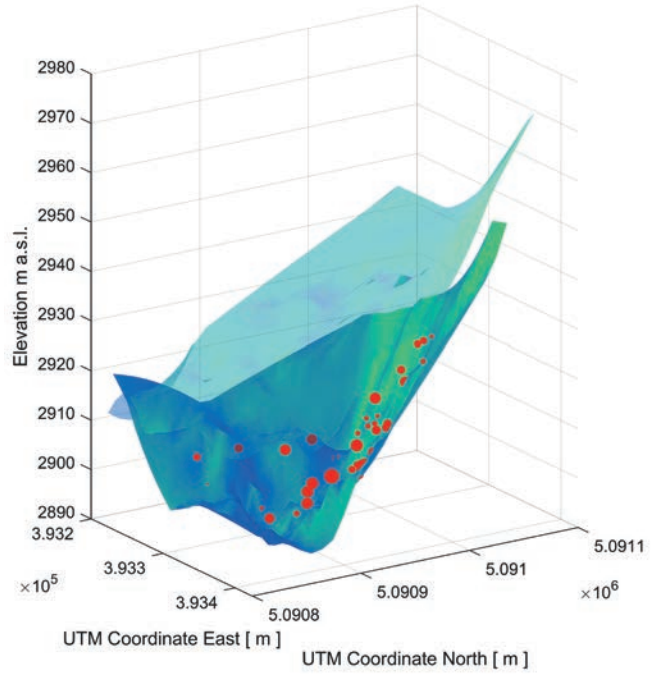

Fig. 5 - 3D rendering of the bedrock morphology according to the interpretation (picking) of the ice-bedrock interface; the upper surface refers to the surface morphology, while the red circles indicate the position of the main georadar artefacts; the size of the circle reflects the relevance of the event.

4. Snow characterisation

In the nivological context, the geophysical approach, adopting seismic and electromagnetic methods, is often used to characterise and monitor of the physical properties and the detection of the free water content of the snowpack. Recent studies have demonstrated how the sudden variations of density and humidity of the snowpack are possible indicators, and at the same time triggering elements, of avalanche phenomena (Jones, 2004). The integration of low-cost devices, such as the water content reflectometer (WCR) sensors (Stein *et al.*, 1997) and georadar, represents a valid technological solution for the seasonal monitoring of the density and snow water content (Godio *et al.*, 2015). The evaluation of these parameters allows estimating the

risk imminence associated with the snow-gliding avalanche release. In such a scenario, seasonal monitoring by means of georadar devices in upward-looking mode (up-GPR) is a consolidated approach to assess these phenomena (Heilig *et al.*, 2009, 2010; Godio *et al.*, 2018). In the up-GPR, the antennas are usually installed on the soil and the radiation is directed upwards with the objective of continuously monitoring the temporal evolution of the seasonal Alpine snowpack and deriving snow stratigraphy information from the radar signals (Schmid *et al.*, 2014).

Georadar investigations are also suitable to evaluate the layering and depositional phenomena of the seasonal snow above the layers of older snow, which is turning into firn and then into ice (e.g. Godio and Rege, 2016). Several methods have been developed to analyse the vertical profiles of seasonal snow and of snow accumulated year by year over the glacial body (Forte *et al.*, 2013, 2014). An example of analysis of snow layering is reported in Fig. 6a; the plot in Fig. 6b refers to a vertical velocity profile obtained by georadar investigation on the Rutor glacier in Aosta Valley, as part of an extensive survey over the glacier to estimate the thickness of the seasonal snow. The main reflectors in radargram of Fig. 6a attest to the presence of the snow-firn layering; particularly, the reflector named A indicates the seasonal snow, the letter B refers to the older snow (previous seasons) which is gradually transforming into firn, while letter C indicates the ice.

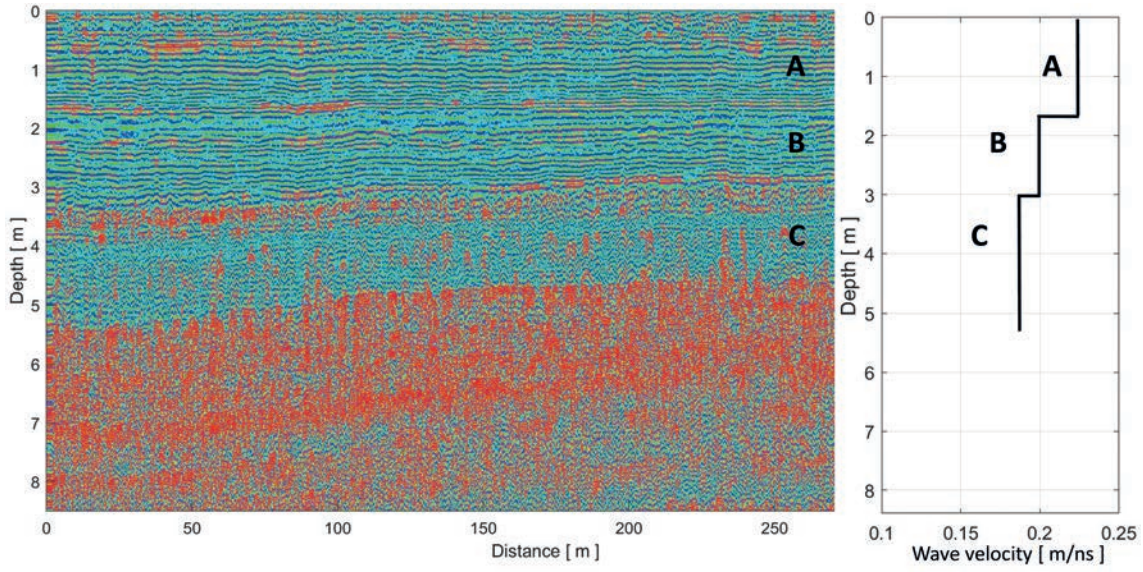

Fig. 6 - Example of radargram to delineate the snow layering and detect layers at different density on the uppermost part of a glacier. In panel a, A indicates the seasonal snow; B refers to the firn or transition between snow and ice, C is the uppermost layer of ice. In panel b, the electromagnetic wave velocities confirm the nature of the layer: higher velocity for the seasonal snow (A) and lower velocity for the uppermost layer of ice (C).

The estimate of electromagnetic wave velocity can be useful to associate the layering to different values of velocity and, hence, to recognise the vertical distribution of density. This is performed by integrating the georadar investigation with other independent measurements, e.g. by using time domain reflectometry or by estimating vertical velocity distribution, inferred by interpreting multiple-offset radar data (e.g. Rege and Godio, 2012; Godio, 2016). The sequence of wave velocity in Fig. 6b shows that: i) the fresh snow is characterised by an average velocity of

0.22-0.23 m/ns, equivalent to a density of about 400-450 kg/m^3; ii) the velocity of the firn is about 0.2 m/ns (density over 600 kg/m^3); iii) the velocity of 0.18 m/ns corresponds to the ice-density of about 800 kg/m^3.

5. Geophysical parameters and mechanical properties of snow/ice

We focus the discussion on some basic aspects referring to seismic and electromagnetic parameters and their relationships with some mechanical properties of snow and ice, basically density and deformability properties.

5.1. Electromagnetic properties of snow

The relationship between density of snow and ice and the electromagnetic wave velocity has been developed in the last 50 years, enabling to estimate with good accuracy the density distribution in depth and to recognise the effect of metamorphism and age of different snow layers. The electromagnetic response of the snow and ice are assimilated to the behaviour of a mixture of fluid and a solid phase. In the following discussion, we neglect the polarisation and depolarisation effects of the electromagnetic field occurring at micro (pore volume, solid grains) and at nanoscale (e.g. water molecules) and we focus on the relationships between electromagnetic properties, density, and free water content.

Studies related to the development of constitutive relationships between geophysical parameters and the physical properties of snow and ice have allowed obtaining increasingly accurate correlations of the hydrological (Sihvola *et al.*, 1985) and mechanical parameters of the snowpack, in order to spatialise the georadar data (Previati *et al.*, 2011) at the various scales, such as slope, catchment or basin.

For dry snow and ice, the relationships between the snow density and the electromagnetic properties are well established; for instance, Robin's equation (Robin, 1975) is an empirical relationship between density and dielectrical permittivity (ε) (Kovacs *et al.*, 1995):

$$\varepsilon = (1 + 0.845 \times \rho)^2 \quad (1)$$

where ρ is the specific gravity of firn and ice (with respect to pure ice) and the dielectrical permittivity is the relative value with respect to the vacuum (dimensionless).

The technical literature reports many variants of mixing models to relate the snow density and dielectric permittivity. Robin's equation is a polynomial fitting of the straightforward Looyenga (1965) formula, which has been widely adopted for computing the dielectric permittivity of a two-phase mixture (ice and gas). A comparison of the validity and drawbacks of different mixing rule are described in Booth *et al.* (2013).

In terms of wave velocity (v) of a radar signal the following relationship holds:

$$v = c / (1 + 0.845 \times \rho) \quad [\text{m/ns}] \quad (2)$$

where c is the wave velocity in vacuum (m/ns). In the velocity range of 0.20 to 0.24 m/ns the specific gravity almost doubles (from 0.3 to 0.6).

The relationship between the radar traveltime (*twt*) of a wave at radiofrequency and the specific gravity becomes:

$$twt = 2 \times d / v \quad [\text{ns}] \tag{3}$$

where d is the snow depth; finally we estimate the Snow Water Equivalent (*SWE*) as:

$$SWE = \rho_{ice} / 2 \times 0.845 \times (c - v) \times twt \quad [\text{kg/m}^3\ \text{m}] \tag{4}$$

The wet snow is a multiphase system compounded by solid matrix (ice), liquid water, and gas. Hence, in a partially saturated medium, the bulk dielectrical permittivity depends upon the fraction of volume occupied by each single phase (fluid and solid) (e.g. Godio, 2008, 2009). A time average equation, based on the general formulation of the CRIM model (Birchak *et al.*, 1974), relates the fraction in volume of the different phases with the bulk dielectrical permittivity (ε):

$$\varepsilon^{\alpha} = (1 - \varphi)\ \varepsilon_i^{\alpha} + \varphi\, S_w\, \varepsilon_w^{\alpha} + (1 - S_w)\ \varphi\, \varepsilon_g^{\alpha} \tag{5}$$

where j is porosity, S_w is the saturation in liquid water while the α-exponent accounts for the structure of the medium; the pedixes *i, w*, and *g* indicate the ice, liquid water, and gas respectively. The porosity of snow ranges between 0.0 (pure ice) to 0.9 (soft snow), saturation is usually lower than 10-20% (for dry snow and pure ice is equal to 0) and the α-exponent is limited in the range between 0.3 and 0.6.

The snowpack is defined in ripe condition when the upper boundary for free water content is equivalent to the maximum volumetric water content (θ_{ret}) that the snowpack can retain against gravity. Therefore, for ripe snow this is dependent from density according to:

$$\theta_{ret} = -0.0745\ (\rho_s / \rho_w) + 0.000267\ (\rho_s / \rho_w)^2 \tag{6}$$

Finally, the snowpack density can be written as:

$$\varphi_s = (1 - \rho)\ \rho_i + \theta\ \rho_w \tag{7}$$

where ρ_i is the ice density (917 kg/m^3), θ is the liquid water content, as the ratio of liquid water volume to total snowpack volume, φ is the porosity, the ratio of pore volume to total snowpack volume. For a typical ripe snowpack of density ρ_s = 500 kg/m^3, θ_{ret} = 0.03.

The density of fresh snow usually ranges between 200-300 kg/m^3; old snow and firn are characterised by values of 500-700 kg/m^3, granular ice and pure ice have density values above 900 kg/m^3. For dry snow up to pure ice, the corresponding values of the dielectrical permittivity (relative) range from 1.5 up to 3.2. A small amount of free water could provide a drastic increase of the dielectrical permittivity (relative).

For a wet snow, with a liquid water content below 10%, the dielectrical permittivity can be related to the density and the water content, according to the following relationship (e.g. Ambach and Denoth, 1980; Godio *et al.*, 2015):

$$\varepsilon_s = 1 + 1.92\rho_{snow} + 0.44\rho_{snow}^{\ 2} + 0.187\theta_w + 0.0045\theta_w^{\ 2} \quad (8)$$

where ε_s is the dielectric permittivity of the snow, ρ_{snow} (g/cm^3) and θ_w (%) are density and water content, respectively.

The sensitivity of dielectrical permittivity to water content can be estimated by applying the Eq. 8; for example, an increase of about 3-5% of the liquid content provides an increase of the dielectrical permittivity of more than 25-35% (e.g. Godio, 2016).

5.2. Mechanical properties of snow and ice

As the mechanical properties of snow and ice play an important role in the snow avalanche risk assessment, we summarise the relationships between the mechanical properties and the geophysical parameters. Elasticity properties of polycrystalline ice have been assessed by several authors (e.g. Sinha, 1989).

The density of ice can be deduced from the fact that there are four molecules per unit cell (Schulson and Duval, 2009); the density of ice (pure) as a function of temperature under atmospheric pressure has been deduced by Hobbs (1974) and it ranges from 916 kg/m^3 at 0 °C to 922 kg/m^3 at -60 °C. The increase of the pressure on the ice determines an increase of the density (Gagnon *et al.*, 1988).

The snow and ice (bulk) density are related to the seismic wave velocity according to the following relationships, valid for porous material and assuming an elastic behaviour:

$$v_p = \sqrt{\frac{K_{sat} + \frac{4}{3}G_{sat}}{\rho_{bulk}}} \quad (9)$$

$$v_s = \sqrt{\frac{G_{sat}}{\rho_{bulk}}} \quad (10)$$

where the bulk compressional modulus K_{sat} (in saturated condition) is related to the mechanical properties of each single constitutive element (liquid water, ice, gas) of the snow and ice according to the Gassmann model.

The Poisson coefficient is computed according to the following formula:

$$\sigma = \frac{V_p^2 - 2V_s^2}{2\left(V_p^2 - V_s^2\right)} \quad (11)$$

The snow or ice bulk density is the named apparent density; it considers the overall volume of the material, including the pore volume:

$$\rho_{bulk} = \left(1 - \varphi\right)\rho_{ice} + S_w\varphi\,\rho_{water} \quad (12)$$

where φ is the porosity, S_w is the free water content and ρ_{ice} is the density of ice or snow crystal and ρ_{water} is the density of water. The density of gas is herein neglected.

The relationship between seismic velocities and density of firn and ice has been suggested by

Kohnen (1974), and allow us to estimate the density values of snow:

$$\rho(z) = 0.915\left\{1+\left[\frac{Vp_{ice}-Vp(z)}{2.25}\right]^{1.22}\right\}^{-1} \quad (13)$$

where $V_{P,ice}$ is the P-wave velocity in compact ice (herein assumed equal to 3.8 km/s) and $V_P(z)$ is the P-wave velocity depth profile; density is in g/cm^3. The previous equation provides an empirical relationship between the density and the experimentally derived P-wave velocity: it is widely adopted in glaciological studies to estimate the density starting from seismic data (e.g. Booth *et al.*, 2013). On the other hand, the P-wave velocity can be predicted considering Gassmann's equations (e.g. Berryman, 2009), relating dry or drained bulk elastic constants to those for fluid-saturated and undrained conditions. Gassmann's equations represent the lower frequency limit of Biot's more general equations of motion for poroelastic materials. The approach does not consider any chemical interactions between the fluids and the solids; moreover, the porosity of the medium remains constant during the saturation or desaturation process. The model states that the compressional modulus in saturated conditions depends on the porosity (φ), the modulus of the fluid filling the pore volume (K_f), to the modulus of the frame in drained conditions (K_{dry}) and the modulus of the snow and ice crystal (K_0):

$$K_{sat} = K_{dry} + \frac{\left(1+\frac{K_{dry}}{K_0}\right)^2}{\left(\frac{\varphi}{K_f}+\frac{1-\varphi}{K_0}-\frac{K_{dry}}{K_0^2}\right)} \quad (14)$$

As the fluid content does not affect the shear deformability of medium, the shear modulus in saturated condition is equal to the one in drained conditions:

$$G_{sat} = G_{dry} \quad (15)$$

One of the more challenging issues of the Gassmann's model is to estimate the mechanical properties of the medium in drained conditions to the mechanical properties of the solid frame (K_0). For consolidated sediments, the relationships between the properties of the grains (K_0 and G_0) and the skeleton properties are given by the following equations:

$$K_{dry} = (1 - D\,\varphi)^2\, K_0 \quad (16)$$

$$G_{dry} = (1 - D\,\varphi)\, G_0 \quad (17)$$

where D is an empirical parameter that could range between 1.5 and 1.9. Assuming a D-value equal to 1.63, a good fit between the Kohnen and the Gassmann model is achieved (Fig. 7).

The predicted wave velocity versus ice density is shown in Fig. 7; the model assumes snow/ice without liquid water content. The bulk or apparent density can be estimated according to Eq. 12: for a pore volume fully saturated by air, the second part of the right term of the equation is neglected.

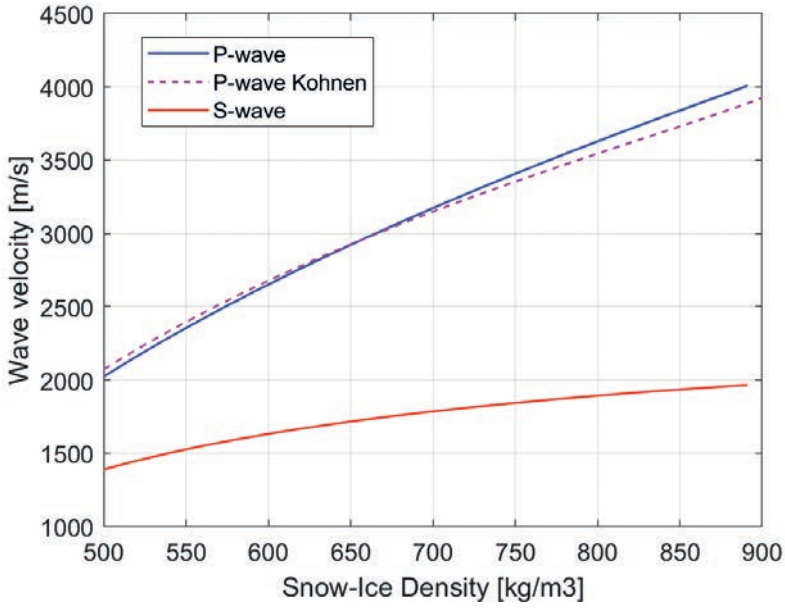

Fig. 7 - Modelling of the P-wave and S-wave wave velocities for different values of snow density; the values achieved with the empirical equation of Kohnen are compared with the values of Gassmann's equations (refer to the text for details); a good fitting (P-wave velocity) of the two theoretical responses is obtained for a coefficient *D* equal to 1.63 (see Eq. 16).

The mechanical bulk compressional modulus of air at standard temperature is equal to 140 kPa. This value is the K_f appearing in Eq. 13. Eqs. 15 and 16 are adopted to estimate the K_{dry} and G_{dry} for a porosity ranging between 0.45 (snow/firn) and 0 (sound or compact ice). The bulk moduli in saturated conditions, K_{sat} and G_{sat} respectively, are computed according to Eqs. 13 and 14; finally, the wave velocities are computed using Eqs. 10 and 11. The K_0 and G_0 are the mechanical properties of the pure ice (e.g. 10.0 and 3.5 GPa, respectively).

As far as the Poisson ratio is concerned, Salm (1971) and Scapozza and Bartelt (2003) referred to values of Poisson ratio in the range of 0.20-0.35 as density increases from 400 to 900 kg/m^3.

King and Jarvis (2007) stated maximum values in the order of 0.34 near the firn/ice transition, while Godio and Rege (2016) reported values in the order of 0.40. It should be noted that the values estimated by Godio and Rege (2016) refer to measurements in the Alpine region at elevations above 3,000 m a.s.l., while King and Jarvis (2007) refer to a glacier in Antarctica. The difference between the two results can be attributed to a different distribution of liquid water that in a temperate glacier could imply a higher ratio of P-wave over S-wave velocities with an increase of the Poisson ratio.

5.3. An example of data interpretation

An example of integration of P and S-wave investigation to estimate the mechanical properties of the uppermost part of the glacier, including the seasonal snow cover and the firn is given by Godio and Rege (2016). They assumed a gradual increase of the P-wave velocity with depth, which causes a continuous refraction of seismic waves curving the ray-path propagation in the uppermost layer of the glacier. Waves propagating in such a way are called diving waves. This assumption, albeit not correct at the small scale, is a good approximation at the scale of the seismic investigation, intended at the wavelength of metres or decades of metres (Kirchner and Bentley, 1990; King and Jarvis, 2007). Starting from the data set of a standard refraction survey,

the P-wave velocity profile is derived adopting the procedure proposed by King and Jarvis (2007), based on the Herglotz-Wiechert formula (Aki and Richards, 2002).

The first arrivals of seismic waves are interpreted as proposed by Kirchner and Bentley (1990), by fitting the travel times with an exponential function:

$$t = a_1 [1 - \exp(-a_2 x)] + a_3 [1 - \exp(-a_4 x)] + a_5 x \quad (18)$$

where t is the first arrival time, x is the source-receiver offset, a_1 to a_4 are constants and a_5 is the minimum slowness recorded in the data. The compressional velocity-depth profiles are computed by deriving analytically the exponential function in Eq. 16, then the curve is converted to a velocity-depth profile by applying the integral formula of Wiechert, Herglotz and Bateman (WHB integral), as discussed in Greenhalgh and King (1980).

The S-wave velocity profiles were achieved by analysing the dispersive characteristics of the surface waves (basically Rayleigh waves): according to the variation of the snow and ice properties with depth, the Rayleigh waves are dispersive, and the phase-velocity is a function of the frequency.

The dispersion curves describe the relationship between the frequency and the phase-velocity. As the dispersion curves depend upon the subsurface geometry and distribution of the mechanical properties, the shear wave velocity can be derived by analysing the dispersive events. Other authors have adopted the dispersive behaviour of seismic waves; Diez *et al.* (2016) inverted the Love and Rayleigh wave dispersion curves to obtain the shear wave velocity profile within the firn and ice to ~150 m depth. The separate inversion of Rayleigh and Love wave dispersion curves evidenced different shear wave velocity profiles within the firn: this difference is attributed to an effective anisotropy due to fine layering.

The dispersion of surface waves on multilayered media is computed according to the Haskell (1953) method. In particular, the approach fixes the P-wave velocity, the density, and the thickness values for each layer, and allows computing the S-wave velocity. The dispersion curves of the surface wave are, then, inverted in order to retrieve the shear waves velocity. The Montecarlo procedure provides a series of statistically reliable 1D models of the snow and ice layering; we refined the solution by applying a deterministic inversion based on a least squares minimisation (e.g. Piatti *et al.*, 2010).

We have applied the aforementioned approach in an Alpine glacier in north-eastern Italy (Pré de Bar glacier, Mont Blanc massif) to retrieve the vertical distribution of the P and S-wave velocity of snow/firn/ice; the results are given in Fig. 8. Note the gradual increase with depth of the velocities, related to the densification process of the snow from the surface to the firn zone.

The selected example comes from a seismic survey on the Pré de Bar glacier in the Aosta Valley, where an integrated refraction P-wave survey and surface wave data acquisition have been performed. The results (Fig. 8) show a smooth and gradual increase of both the P-wave and S-wave vertical velocity profiles. At the maximum achieved depth (about 35 m), a P-wave velocity of about 3700 m/s and a S-wave velocity of about 1500 m/s have been observed. Some differences from the results reported by other authors can be noticed: e.g. Picotti *et al.* (2017) reported a maximum value of the S-wave velocity of about 1860 m/s on the Pian di Neve glacier (eastern Alps, Adamello massif), even if they referred to a low-altitude glacier where the snow densification process is usually very sharp and, therefore, the velocity gradients are sharp as well.

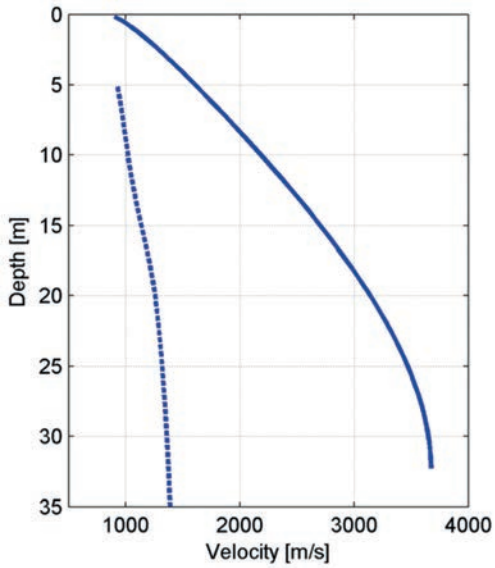

Fig. 8 - Example of vertical distribution of P-wave and S-wave velocity on the uppermost part of an Alpine glacier.

At higher elevations (more than 3000 m a.s.l.), as in the Pré de Bar glacier, the densification process follows a more gradual behaviour and the thickness of the firn transitional zone could be higher. However, because of a non-optimised surface wave configuration during the data acquisition, we had to force the interpretation of the shear wave in order to obtain the same depth of investigation that has been achieved by the P-wave interpretation. This yields a lack of resolution of the vertical velocity distribution at depth greater than 25 m and a probable underestimation of the S-wave velocity at deeper layers. Moreover, S-waves are insensitive to pore fluid; they are sensitive to the properties of the grains (or, in our case, the snow crystals). By contrast, P-waves are highly affected by changes in pore fluid [i.e. residual liquid water in the snow; Schweizer (2002)]. As there is a highly nonlinear relationship between velocity and water saturation, the presence of free water could strongly affect the distribution of the P-wave velocity, while S-wave velocity is not affected at all. More generally, in most Alpine glaciers at high elevation (higher than 3,000 m a.s.l.), we observe a slight and gradual increase of the bulk compressional modulus from about 1 GPa at 5 m of depth to about 10.0-10.5 GPa at 25 m; the shear modulus ranges from about 0.4 to 1.7 GPa. In many cases, the lack of temperature measurements of the snow does not allow us to account for the temperature effect on the shear modulus (Schweizer and Camponovo, 2002).

6. Conclusions

We have highlighted the application of geophysical methods for the characterisation of snow and glacial systems in high-altitude Alpine environments, in order to estimate the hazard related to recent deglaciation phenomena. The most recent developments aim at characterising the discontinuities and the cavities inside the glacial masses, which can give rise to collapses with the release of large amounts of water. Integrated methodologies are required to characterise and monitor the physical properties of the snowpack (both seasonal snow and in glacial ice storage basins). We have discussed some models to predict the density from the observed geophysical

parameters. The suggested models do not consider a multiphase pore fluid (i.e. both air and liquid water within pore spaces). In the GPR case, the effect of liquid water would be to reduce the propagation velocity, with an overestimate of density. In the seismic case, the highly nonlinear relationship between velocity and water saturation provides a more challenging prediction of the effect of liquid water on a density estimate.

The efficiency of GPR acquisitions has been widely demonstrated to effectively estimate the snow cover depth and and/or the ice thickness. However, the acquisition of CMP data is necessary for velocity analysis, to improve the resulting accuracy of depth conversions.

Seismic acquisitions are much less efficient than GPR, but may provide an accurate evaluation of the density and other bulk mechanical properties (elastic moduli): this requires the integration of P-wave data acquisition with S-wave investigation. The acquisition of surface waves represents an effective way to estimate the shear wave velocity distribution, even if an optimal design of the survey is required to investigate through the snow/firn transitional zone.

In such a scenario, the main interest of the stakeholders is to develop lighter devices for monitoring over wide areas at low costs. Lidar and other geomatic devices are already available for installation on cost-effective drones, while geophysical sensors still require some work to minimise weights and logistical issues of installation.

Snow characterisation in the avalanche risk analysis will require new integrated monitoring devices to characterise mechanical parameters, density and snow humidity. At the same time, cost effective new technologies are needed in avalanche warning at the scale of slope and catchment.

The development of highly sensitive optical sensors represents a fascinating but challenging field of novelty. They are able to monitor pressure, temperature and deformation that can be related to density, humidity and mechanical behaviour of the snow cover. The application of distributed temperature sensors (DTS) and distributed acoustic sensors (DAS) is still a frontier in glaciological studies, because of the high investment costs of the tools for monitoring large areas.

Acknowledgements. The author is grateful to the Scientific Committee of GNGTS 2017 for the invitation to present the topic as a keynote of the Session of Applied Geophysics. Dario Slejko has demonstrated patience, competence, and professionalism during all the editorial process. The author appreciated the useful comments and suggestions made by the two reviewers. Their valuable work allowed improving the quality of the manuscript.

REFERENCES

Aki K. and Richards P.G.; 2002: *Quantitative Seismology, 2nd ed*. University Science Books, 704 pp.

Ambach W. and Denoth A.; 1980: *The dielectric behaviour of snow: a study versus liquid water content.* In: Proc. NASA Workshop, Microwave Remote Sensing of Snowpack Properties, Fort Collins, CO, USA, pp. 69-92.

Arcone S.A.; 1996: *High resolution of glacial ice stratigraphy: a ground-penetrating radar study of Pegasus Runway, McMurdo Station, Antartica*. Geophys., **61**, 1653-1663.

Arcone S.A., Lawson D.E. and Delaney A.J.; 1995: *Short-pulse radar wavelet recovery and resolution of dielectric contracts within englacial and basal ice of Matanuska Glacier, Alaska, USA*. J. Glaciol., **41**, 68-86.

Arcone S.A., Lawson D.E., Delaney A.J., Strasser J.C. and Strasser J.D.; 1998: *Ground-penetrating radar reflection profiling of groundwater and bedrock in an area of discontinuous permafrost*. Geophys., **63**, 1573-1584.

Berryman J.; 2009: *Origins of Gassmann's equations*. Geophys., **64**, 1627-1629, doi: 10.1190/1.1444667.

Birchak J.R., Gardner C.G., Hipp J.E. and Victor J.M.; 1974: *High dielectric constant microwave probes for sensing soil moisture.* In: Proc. IEEE, 670 62, pp. 93-98, doi: 10.1109/PROC.1974.9388.

Bohleber P., Sold L., Hardy D.R., Schwikowski M., Klenk P., Fischer A., Sirguey P., Cullen N.J., Potocki M., Hoffmann H. and Mayewski P.; 2017: *Ground-penetrating radar reveals ice thickness and undisturbed englacial layers at Kilimanjaro's northern Ice Field*. The Cryosphere, **11**, 469-482, doi: 10.5194/tc-11-469-2017.

Booth A.D., Mercer A., Clark R., Murray T., Jansson P. and Axtell C.; 2013: *A comparison of seismic and radar methods to establish the thickness and density of glacier snow cover*. Ann. Glaciol., **54**, 73-82, doi: 10.3189/2013aog64a044.

Carturan L., Baroni C., Becker M., Bellin A., Cainelli O., Carton A., Casarotto C., Dalla Fontana G., Godio A., Martinelli T., Salvatore M.C. and Seppi R.; 2013: *Decay of a long-term monitored glacier, the Careser Glacier (Ortles-Cevedale, European Alps).* The Cryosphere, **7**, 1819-1838, doi: 10.5194/tc-7-1819-2013.

Colgan W., Rajaram H., Abdalati W., McCutchan C., Mottram R., Moussavi M.S. and Grigsby S.; 2016*: Glacier crevasses: observations, models, and mass balance implications*. Rev. Geophys., **54**, 119-161, doi: 10.1002/2015RG000504.

Diez A., Bromirski P.D., Gerstoft P., Stephen R.A., Anthony R.E., Aster R.C., Cai C., Nyblade A. and Wiens D.A.; 2016: *Marine geosciences and applied geophysics ice shelf structure derived from dispersion curve analysis of ambient seismic noise, Ross Ice Shelf, Antarctica*. Geophys. J. Int., **205**, 785-795, doi: 10.1093/gji/ggw036.

Diolaiuti G.A., Maragno D., D'Agata C., Smiraglia C. and Bocchiola D.; 2011: *Glacier retreat and climate change: documenting the last 50 years of Alpine glacier history from area and geometry changes of Dosde Piazzi Glaciers (Lombardy Alps, Italy).* Prog. Phys. Geogr., **35**, 161-182.

Eisen O., Nixdorf U., Keck L. and Wagenbach D.; 2003: *Alpine ice cores and ground penetrating radar: combined investigations for glaciological and climatic interpretations of a cold Alpine ice body*. Tellus Ser B, **55**, 1007-1017.

Eisen O., Hamann I., Kipfstuhl S., Steinhage D., Wilhelms F.; 2007: *Direct evidence for continuous radar reflector originating from changes in crystal-orientation fabric.* The Cryosphere **1**, 1-10.

Ferrero A., Godio A., Migliazza M., Sambuelli L., Segalini A. and Theodule A.; 2014: *Geotechnical and geophysical characterization of frozen granular material*. In: Shan W., Guo Y., Wang F., Marui H. and Strom A. (eds), Landslides in Cold Regions in the Context of Climate Change, Springer International Publishing, Berlin, Germany, pp. 205-218.

Fischer A. and Kuhn M.; 2013: *Ground-penetrating radar measurements of 64 Austrian Glaciers between 1995 and 2010*. Ann. Glaciol., **54**, 179-188.

Forte E., Dossi M.,Colucci R.R. and Pipan M.; 2013: *A new fast methodology to estimate the density of frozen materials by means of common offset GPR data*. J. Appl. Geophys., **99**, 135-145, doi: 10.1016/j.jappgeo.2013.08.013.

Forte E., Dossi M., Pipan M. and Colucci R.R.; 2014: *Velocity analysis from common offset GPR data inversion: theory and application to synthetic and real data*. Geophys. J. Int., **197**, 1471-1483.

Forte E., Pipan M., Francese R. and Godio A.; 2015: *An overview of GPR investigation in the Italian Alps*. First Break, **33**, 61-67.

Francese R.G., Bondesan A., Giorgi M., Picotti S., Carcione J.M., Baroni C., Salvatore M.C. and Nicolis F.; 2019: *Geophysical signature of a world war I tunnel in the Forni Glacier (Punta Linke, Italian Alps)*. J. Glaciol., **65**, 798-812, doi:10.1017/jog2019.59.

Frey H., Haeberli W., Linsbauer A., Huggel C. and Paul F.; 2010: *A multi-level strategy for anticipating future glacier lake formation and associated hazard potentials*. Nat. Hazards Earth Syst. Sci., **10**, 339-352.

Gagnon R.E., Kiefte H., Clouter M.J. and Whalley E.; 1988: *Pressure dependence of the elastic constants of ice Ih to 2.8 kbar by Brillouin spectroscopy*. J. Chem. Phys., **89**, 4522-4528.

Garambois S., Legchenko A., Vincent C. and Thibert E.; 2016: *Ground-penetrating radar and surface nuclear magnetic resonance monitoring of an englacial water-filled cavity in the polythermal glacier of Tête Rousse*. Geophys., **81**, WA131-WA146, doi: 10.1190/geo2015-0125.1.

Godio A.; 2008: *Performance and experimental evidence of GPR in density estimates of snowpack*. Boll. Geof. Teor. Appl., **49**, 279-298.

Godio A.; 2009: *Georadar measurements for snow cover density*. Am. J. Appl. Sci., **6**, 414-423.

Godio A.; 2016: *Multi population genetic algorithm to estimate snow properties from GPR data.* J. Appl. Geophys., **131**, 133-144.

Godio A. and Rege R.B.; 2015: *The mechanical properties of snow and ice of an alpine glacier inferred by integrating seismic and GPR methods*. J. Appl. Geophys., **115**, 92-99.

Godio A. and Rege R.B.; 2016: *Analysis of georadar data to estimate the snow depth distribution.* J. Appl. Geophys., **129**, 92-100, doi: 10.1016/j.jappgeo.2016.03.036.

Godio A., Franco D., Chiaia B., Frigo B., Dublanc L., Freppaz M., Maggioni M., Ceaglio E. and Dellavedova P.; 2015: *Seasonal monitoring of snow properties by WCR and up-GPR*. In: Extended Abstract, 21st European Conference, Near Surface Geoscience 2015, Torino, Italy, 4 pp., doi: 10.3997/2214-4609.201413721.

Godio A., Frigo B., Chiaia B., Maggioni M., Freppaz M., Ceaglio E. and Dellavedova P.; 2018: *Integration of upward GPR and water content reflectometry to monitor snow properties*. Near Surf. Geophys., **16**, 1-10, doi: 10.3997/1873-0604.2017060.

Greenhalgh S.A. and King D.W.; 1980: *Determination of velocity-depth distribution by inversion of refraction time-distance data*. Explor. Geophys., **11**, 92-98, doi: 10.1071/EG980092.

Haeberli F.; 1983: *Frequency and characteristics of glacier floods in the Swiss Alps*. Ann. Glaciol., **4**, 85-90.

Haskell N.A.; 1953: *The dispersion of surface waves on multilayered media*. Bull. Seismol. Soc. Am., **43**, 17-34.

Heilig A., Schneebeli M. and Eisen O.; 2009: *Upward-looking ground-penetrating radar for monitoring snowpack stratigraphy*. Cold Reg. Sci. Technol., **59**, 152-162, doi: 10.1016/j.coldregions.2009.07.008.

Heilig A., Eisen O. and Schneebeli M.; 2010: *Temporal observations of a seasonal snowpack using upward-looking GPR*. Hydrol. Processes, **24**, 3133-3145, doi: 10.1002/hyp.7749.

Hobbs P.V.; 1974: *Ice physics*. Oxford University Press, Oxford, UK, 856 pp.

Jones A.; 2004: *Review of glide processes and glide avalanche release*. Avalanche News, **69**, 53-60.

King E.C. and Jarvis E.P.; 2007: *Use of shear waves to measure Poisson's ratio in polar firn*. J. Environ. Eng. Geophys., **12**, 15-21, doi: 10.2113/JEEG12.1.15.

Kirchner J.F. and Bentley C.R.; 1990: *RIGS III: seismic short refraction studies using an analytical curve fitting technique*. In: Bentley C.R. and Hayes D.E. (eds), The Ross Ice Shelf: Glaciology and Geophysics, Antarctic Research Series, vol. 42, pp. 109-126.

Kohnen H.; 1974: *On the relationship between seismic velocities and density in firn and ice*. Z. Geophys., **38**, 925-935.

Konrad H., Bohleber P., Wagenbach D., Vincent C. and Eisen O.; 2013: *Determining the age distribution of Colle Gnifetti, Monte Rosa, Swiss Alps, by combining ice cores, ground-penetrating radar and a simple flow model*. J. Glaciol., **59**, 179-189.

Kovacs A., Gow A.J. and Morey R.M.; 1995: *The in-situ dielectric constant of polar firn revisited*. Cold Reg. Sci. Technol., **23**, 245-256.

Künzler M., Huggel C., Linsbauer A. and Haeberli W.; 2010: *Emerging risks related to new lakes in deglaciating areas of the Alps*. In: Malet J.-P, Glade T. and Casagli N. (eds), Mountain Risks: Bringing Science to Society, Proc. of the 'Mountain Risk' International Conference, Firenze, Italy, pp. 453-458.

Legchenko A., Ezersky M., Camerlynck C., Al-Zoubi A., Chalikakis K. and Girard J-F.; 2008: *Locating water-filled karst caverns and estimating their volume using magnetic resonance soundings*. Geophys., **73**, G51-G61, doi: 10.1190/1.2958007.

Legchenko A., Descloitres M., Vincent C., Guyard H., Garambois S., Chalikakis K. and Ezersky M.; 2011: *Three-dimensional magnetic resonance imaging for groundwater*. New J. Phys., **13**, 025022, doi: 10.1088/1367-2630/13/2/025022.

Legchenko A., Vincent C., Baltassat J.M., Girard J.F., Thibert E., Gagliardini O., Descloitres M., Gilbert A., Garambois S., Chevalier A. and Guyard H.; 2014: *Monitoring water accumulation in a glacier using magnetic resonance imaging*. The Cryosphere, **8**, 155-166, doi: 10.5194/tc-8-155-2014.

Looyenga H.; 1965: *Dielectric constants of heterogeneous mixtures*. Phys., **31**, 401-406.

Mercalli L., Cat Berro D., Mortara G. and Tamburini A.; 2002: *Un lago sul ghiacciaio del Rocciamelone, Alpi Occidentali: caratteristiche e rischio potenziale*. NIMBUS, **23-24**, 3-9.

Moore P., Winberry J., Iverson N., Christianson K., Anandakrishnan S., Jackson M., Mathison M. and Cohen D.; 2013: *Glacier slip and seismicity induced by surface melt*. Geol., **41**, 1247-1250, doi: 10.1130/G3470.1.

Mortara G. and Mercalli L.; 2002: *Il lago epiglaciale "Effimero" sul ghiacciaio del Belvedere, Macugnaga, Monte Rosa*. NIMBUS, **23-24**, 10-17.

Murray T., Stuart G.W., Fry M., Gamble N.H. and Crabtree M.D.; 2000: *Englacial water distribution in a temperate glacier from surface and borehole radar velocity analysis*. J. Glaciol., **46**, 389-398.

Navarro F.J., Macheret Y.Y. and Benjumea B.; 2005: *Application of radar and seismic methods for the investigation of temperate glaciers*. J. Appl. Geophys., **57**, 193-211.

Piatti C., Boiero D., Godio A. and Socco L.V.; 2010: *Improved Monte Carlo 1D - Inversion of VES and TDEM data*. Near Surf. Geophys., **8**, 117-133, doi: 10.3997/1873-0604.2009055.

Picotti S., Vuan A., Carcione J.M., Horgan H.J. and Anandakrishnan S.; 2015: *Anisotropy and crystalline fabric of Whillans Ice Stream (west Antarctica) inferred from multicomponent seismic data*. J. Geophys. Res., **120**, 4237-4262.

Picotti S., Francese R., Giorgi M., Pettenati F. and Carcione J.M.; 2017: *Estimation of glacier thicknesses and basal properties using the horizontal-to-vertical component spectral ratio (HVSR) technique from passive seismic data*. J. Glaciol., **63,** 229-248, doi: 10.1017/jog.2016.135.

Podolskiy E.A. and Walter F.; 2016: *Cryoseismology*. Rev. Geophys., **54**, 708-758, doi: 10.1002/2016RG000526.

Pomeroy J., Brisbourne A., Evans J. and Graham D.; 2013: *The search for seismic signatures of movement at the glacier bed in a polythermal valley glacier*. Ann. Glaciol., **54**, 149-156, doi: 10.3189/2013AoG64A203.

Pomeroy J.W., Bernhardt M. and Marks D.; 2015: *Water resources: research network to track alpine water*. Nature, **521**, 156-157, doi: 10.1038/521032c.

Previati M., Godio A. and Ferraris S.; 2011: *Validation of spatial variability of snowpack thickness and density obtained with GPR and TDR methods*. J. Appl. Geophys., **75**, 284-293.

Rege R.B. and Godio A.; 2012: *Multimodal inversion of guided waves in georadar data*. J. Appl. Geophys., **81**, 68-75, doi: 10.1016/j.jappgeo.2011.09.021.

Robin G. de Q.; 1975: *Velocity of radio waves in ice by means of a bore-hole interferometric technique*. J. Glaciol., **15**, 151-159, doi: 10.3189/S0022143000034341.

Salm B.; 1971: *On the rheological behaviour of snow under high stresses.* Contributions from the Institute of Low Temperature Science, Hokkaido University, Sapporo, Japan, A23, pp. 1-43.

Scapozza C. and Bartelt P.; 2003: *Triaxial tests on snow at low strain rate. Part II: constitutive behaviour*. J. Glaciol., **49**, 91-101.

Schmid L., Heilig A., Mitterer C., Schweizer J., Maurer H., Okorn R. and Eisen O.; 2014: *Continuous snowpack monitoring using upward-looking ground-penetrating radar technology*. J. Glaciol., **60**, 509-525, doi: 10.3189/2014JoG13J084 509.

Schulson E.M. and Duval P.; 2009: *Creep and fracture of ice*. Cambridge University Press, Cambridge, U.K., 401 pp., doi: 10.1017/CBO9780511581397.

Schweizer J.C.; 2002: *The temperature dependence of the effective elastic shear modulus of snow*. Cold Reg. Sci. Technol., **35**, 55-64.

Schweizer J. and Camponovo C.; 2002: *The temperature dependence of the effective elastic shear modulus of snow.* Cold Regions Science and Technology, **35**, 55-64, doi: 10.1016/S0165-232X(02)00030-7.

Sihvola A., Nyfors E. and Tiuri M.; 1985: *Mixing formulae and experimental results for the dielectric constant of snow*. J. Glaciol., **31**, 163-170.

Sinha N.K.; 1989: *Elasticity of natural type of polycrystalline ice.* Cold Reg. Sci. Technol., **17**, 127-135.

Stein J., Laberge G. and Lèvesque D.; 1997: *Monitoring the dry density and the liquid water content of snow using time domain reflectometry*. Cold Reg. Sci. Technol., **25**, 123-136.

Stoffel M. and Huggel C.; 2012: *Effects of climate change on mass movements in mountain environments.* Prog. Phys. Geog., **36**, 421-439.

Stuart G., Murray T., Gamble N., Hayes K. and Hodson A.; 2003: *Characterization of englacial channels by ground-penetrating radar: an example from austre Brøggerbreen, Svalbard*. J. Geophys. Res., **108**, 2525, doi: 10.1029/2003jb002435.

Tamburini A., Villa A., Villa F., Bruno V. and Frattini P.; 2008: *Indagini Ground Penetrating Radar sul ghiacciaio settentrionale delle Locce (Monte Rosa, Macugnaga). Approccio metodologico e risultati*. In: Proc. 27th Convegno Nazionale, Gruppo Nazionale di Geofisica della Terra Solida, Trieste, Italy, pp. 393-395.

Vincent C., Garambois S., Thibert E., Lefèbvre E., Le Meur E. and Six D.; 2010: *Origin of the outburst flood from Glacier de Tête Rousse in 1892 (Mont Blanc area, France)*. J. Glaciol., **56**, 688-698, doi: 10.3189/002214310793146188.

Vincent C., Descloitres M., Garambois S., Legchenko A., Guyard H. and Gilbert A.; 2012: *Detection of a subglacial lake in Glacier de Tête Rousse (Mont Blanc area, France)*. J. Glaciol., **58**, 866-878, doi: 10.3189/2012JoG11J179.

Zemp M., Haeberli W., Bajracharya S., Chinn T.J., Fountain A.G., Hagen J.O., Huggel C., Kääb A., Kaltenborn B.P., Karki M., Kaser G., Kotlyakov V.M., Lambrechts C., Li Z.Q., Molnia B.F., Mool P., Nellemann C., Novikov V., Osipova G.B., Rivera A., Shrestha B., Svoboda F., Tsvetkov D.G. and Yao T.D.; 2007: *Glaciers and ice caps. Part I: global overview and outlook. Part II: glacier changes around the world.* In: UNEP: global outlook for ice and snow, UNEP/GRID-Arendal, Norway, pp. 115-152.

Corresponding author: Alberto Godio
Dipartimento di Ingegneria dell'Ambiente, del Territorio e delle Infrastrutture (DIATI),
Politecnico di Torino
Corso Duca degli Abruzzi 24, 10129 Torino, Italy
Phone: +39 011 0907656; e-mail: alberto.godio@polito.it